Research Article

Mathematical Methods in the Applied Sciences

Received XXXX

(www.interscience.wiley.com) DOI: 10.1002/sim.0000
MOS subject classification: 37C27; 37C29; 37C80

Deriving phase-response curves of ion channel gating kinetics

Jan-Hendrik Schleimer*, Susanne Schreiber

Reduced models of single-neuron dynamics are widely used to characterize neuronal properties, encoding, and a cell's contribution to network function. Low-dimensional phase oscillator models based on phase-response curves, in particular, permit to capture the essence of a neuron's input-output dynamics at the level of spike times from high-dimensional conductance-based neuron models. In principle, these phase models allow for a direct translation of perturbations in the state variables (such as changes in specific ion channel conductances and kinetics) to shifts in the timing of spikes. Previous mathematical work, however, has predominantly focused on voltage and current perturbations and less on perturbations occuring in any of the involved kinetic equations of ionic channels. Here, we provide the means to mathematically relate properties in these variables to the phase-dependent voltage dynamics. Specifically, we derive the vector of phase-response curves near two different onset bifurcations: the physiologically prominent saddle-node on invariant cycle bifurcation as well as the saddle-node loop bifurcation. We demonstrate that, locally around the saddle-node, the tangent space of the isochrons is spanned by the strongly-stable manifold of the saddle-node. This finding enables us to quantitatively relate perturbations in the gating kinetics of ion channels to the resulting changes in spike timing. These results lay the methodological foundation for future quantitative analyses of the impact of specific biophysical channel properties on spike timing, including but not limited to channel noise.

Keywords: saddle-node loop; saddle-node on invariant cycle; homoclinic-orbits to a saddle-node; isochrones; phase-response curves; conductance-based neuron model; gating kinetics; semi-stable manifold; strongly-stable manifold

Introduction

A neuron's membrane voltage is constantly subject to fluctuations induced by perturbations of its ionic conductances[1–4]. Consequently, such perturbations (of both synaptic or cell-intrinsic origin) modulate the membrane voltage and interfere with action potential generation, resulting in the cancellation, production, or a shift in the timing of spikes[5,6]. Such perturbations are known to affect a neuron's information processing capabilities[7,8] as well as to impact normal and pathological dynamics of neuronal ensembles[9,10].

While perturbations to the gating kinetics of ion channels have been described and quantified on the level of voltage fluctuations[11,12], a systematic approach towards a quantitative prediction of the impact of perturbations in a given channel type on spike timing is currently lacking. Given the huge molecular and functional variety of ion channels and postsynaptic ion-conducting receptors (the number of potassium channel genes alone exceeds 60) as well as their important role in pathology and health, we need to characterize the susceptibility of spike timing to perturbations in ion channel kinetics. To construct a mathematical relation between ion channel kinetics in a broad biophysical class of single neuron models (i.e.,

Institute for Theoretical Biology, Humboldt University, Philippstraße 13, Haus 4, 10115 Berlin, Germany
** Correspondence to: jh.schleimer@hu-berlin.de*

conductance-based models) and spike timing jitter for neurons driven in a regular firing mode (i.e., in the presence of an invariant cycle representing the spike), phase-response curves for the gating variables of ion channels are an adequate means. In this article, analytical expressions for the gating phase-response curves are derived. This opens up the possibility for an efficient, quantitative, and channel-specific impact analysis of biophysical properties on neuronal firing.

Our specific approach is based on the phase-response curves and isochrones of the neuronal oscillator. Phase-response curves characterize the temporal shift induced by a perturbation on the timing of the next spike as a function of the phase at which the perturbation was presented. Isochrones characterise sets of initial conditions in the state space that result in the same phase. To relate perturbations in the ion channels' gating variables to spike timing (i.e., the phase of the oscillation), we here exploit the fact that phase-response curves are the normal to the isochrones' tangent space, see *Corollary 2*. The shapes of the phase-response curves are derived from a centre-manifold reduction of the dynamical system, *cf. Observation 4*. The relative scaling between the system's variables is obtained by considering that – for a specific point on the limit cycle – the tangent space of the isochrones is spanned by the strongly stable directions of eigensystem at the saddle-node, see *Conjecture 6*. We further demonstrate that the peak of the phase-response curve remains close to the ghost of the saddle-node. Taken together, global information on the phase-response of all gating variables can thus be obtained from the zeroth eigenvector of the Jacobian at the saddle-node, which for conductance-based neurons is given analytically in *Observation 5*. Our analysis hence provides analytical access to all the ingredients required for a quantitative mapping of perturbations in any system variable to the resulting phase of the voltage oscillation, i.e. spike timing (see *Corollary 8*).

In this article, we first define the model, including its phase-reduction, and outline the general assumptions. Next, the general spike-onset bifurcations considered here are introduced. Thereafter, a brief introduction to isochrones and phase-response curves (PRCs) is given, followed by the core results: the calculation of PRCs for specific onset-bifurcations.

General assumptions for conductance-based neuron model and their phase-reductions

The voltage dynamics at a neuron's membrane is commonly described by a current-balance equation, which for large ion channel densities is accompanied by $n-1$ first-order kinetic rate equations (reaction-rate theory) for the gating activity of the voltage-gated ion channels[13].

Def. 1 *(Conductance-based neuron model)*

In a conductance-based neuron model, the evolution of the membrane voltage, $v \in \mathbb{R}$, and the kinetic variables $a_k \in [0,1] \subset \mathbb{R}$, describing the fraction of open ion channel gates (or synaptic gates), have the following form

$$(1)\quad \begin{aligned} \frac{\mathrm{d}v}{\mathrm{d}t} &= (I_{\mathrm{in}} + I_{\mathrm{ion}}(v, \{a_k\}_{k=1}^{n-1}))/C_{\mathrm{m}}, \\ \frac{\mathrm{d}a_k}{\mathrm{d}t} &= (a_k^{(\infty)}(v) - a_k)/\tau_k(v), \end{aligned},$$

where I_{in} denotes the applied stimulus and C_{m} the membrane capacitance. The functions $a_k^{(\infty)}(v)$ and $\tau_k(v)$ are the twice-differentiable steady-state activation curve, and time constant, of the k^{th} gate respectively. The ionic currents generated by the ion channels in the membrane are

$$I_{\mathrm{ion}} = \sum_{i=1}^{m} g_i(a_{h_i}, ..., a_{(h_{i+1})-1})(E_i - v).$$

E_i represents the i^{th} ion channel's Nernst potential. The function, $g_i : \mathbb{R}^{\ell_i} \mapsto [0, g_i^{\max}] \subset \mathbb{R}$, represents the ion channel's conductance that depends on ℓ_i gating variables. As each channel has ℓ_i gates, the gates' indices are $h_1 = 1$ and $h_i = \sum_{j=1}^{i} \ell_j \; \forall i > 0$. The total number of ion channels in the membrane is m.

For brevity, define the state vector $\vec{x} = [v, a_1, ..., a_{n-1}]^\top \in \mathbb{R}^n$ to be composed of the voltage dimension and $n-1$ kinetic variables. The unperturbed, autonomous system from Eq. (1) is then denoted as

$$(2)\quad \dot{\vec{x}} = \vec{F}(\vec{x}).$$

In addition, let $\vec{\eta}(\vec{x}, t)$ be an infinitesimal perturbation to the r.h.s. of Eq. (2), such that

$$(3)\quad \dot{\vec{x}} = \vec{F}(\vec{x}) + \vec{\eta}(\vec{x}, t).$$

The following desiderata are placed, which will enable us to consider a widespread class of excitability in conductance-based neuron models, corresponding to particular onset-bifurcations and, most importantly, requiring the existence of a saddle-node with homoclinic orbits attached to it.

Assumption #ass:invariantcycle (i) *Tonic spiking*: Let the neuron's resting state vanish in an saddle-node bifurcation at some parameter $I_{\mathrm{in}} = I_{\mathrm{sn}}$. Then, for $I_{\mathrm{in}} > I_{\mathrm{sn}}$, Eq. (2) is assumed to have a $T_{\mathrm{p}}(I_{\mathrm{in}})$-periodic hyperbolic invariant cycle (ic) attractor, denoted $\vec{x}_{\mathrm{ic}}(t)$, with $\vec{x}_{\mathrm{ic}}(t) = \vec{x}_{\mathrm{ic}}(t + T_{\mathrm{p}}(I_{\mathrm{in}}))$. (ii) *Low firing rates*: This allows us to inspect the limit $T_{\mathrm{p}} \to \infty$. Neurons that can spike at arbitrarily low firing rate are sometimes called type I neurons or are said to have class I excitability[14]. More precisely, it is required that the period of the neuron is long compared to all other time-scales of the system. Low firing rates are, *e.g.*, observed for cortical pyramidal neurons. (iii) *All-or-none law*: The amplitude of an action potential is independent of the strength of the perturbation that caused it. (iv) *No bistability*: Prudently, the neuron is assumed to show no bistability, which rids us of phaseless sets in the vicinity of the invariant cycle dynamics.

Assumption 1

As in all conductance-based neuron models, the steady-state activation curves are assumed to be strictly monotonous (sigmoidal) functions $\forall v : \frac{\mathrm{d}}{\mathrm{d}v} a_k^{(\infty)}(v) \neq 0$.

Injected-current perturbations will affect the voltage dimension of $\vec{x}$. Many perturbations from biological processes, however, affect the kinetic equations. Such biological sources may include synaptic activity[15] or the ion channel kinetics themselves[16–18] and are viewed as a perturbation to the deterministic part of the dynamics, $\vec{x}_{\mathrm{ic}}(t)$.

The mathematical description of neuronal dynamics above the rheobase (threshold), where tonic firing of action potentials (spikes) commences, can rely on the existence of invariant cycles (or limit cycles) with an asymptotic phase variable and a period T_{p}[19]. To study the statistics of the event series of spike times $\{t_k^{\mathrm{sp}}\}$, it is convenient to define the phase variable, $\phi \in \mathbb{R}$, such that $\phi(t_k^{\mathrm{sp}}) = k, \forall k \in \mathbb{Z}$, see *Fig. 1*. In general, the dynamics in the limit cycle's basin of attraction can be completely described by a phase-amplitude model[20]. If the invariant cycle is stiff, *i.e.*, its Floquet exponents are sufficiently negative compared to the perturbation strength to guarantee convergence to the invariant cycle within one period, a phase-only equation describes the dynamics of spike times well[21,22]:

$$(4)\quad \dot{\phi} = \vec{\nabla}\phi \cdot \frac{\mathrm{d}\vec{x}}{\mathrm{d}t} = f_0 + \vec{\nabla}\phi \cdot \vec{\eta}(t) + \text{ h.o.t.}$$

Here, the vector $\vec{\eta} \in I\!R^n$ subsumes all sources of perturbations from both the voltage and the kinetic equations of all the ion channel gates that contribute to the voltage dynamics. If the unperturbed system has an *invariant cycle* solution, the phase gradient $\vec{\nabla}\phi$ is normalised such that it equals the constant firing rate $f_0 = \vec{\nabla}\phi \cdot \vec{x}_{\mathrm{ic}}$. If the phase gradient is calculated from a neuron model, the phase equation, Eq. (4), can act as an input-output equivalent spike encoder[23], see *Fig. 1* for an example.

Perturbing currents that directly influence the voltage dimension, *e.g.* from a stimulating electrode, have been studied previously[24,25]. Yet, many perturbations impinge on the kinetic equations describing the gating of Ohmic-conductances in the membrane. Other neurons may perturb synaptic conductances and intrinsic channel noise may result from finite-size effects in the number of ion channels. Therefore, this article derives the complete vector of phase-response curves for a neuron with specific spike-onset bifurcations, *i.e.*, mechanisms to change from resting to spiking behaviour. In particular, the saddle-node on invariant cycle (SNIC) and saddle-node loop (SNL) bifurcations are considered.

In order to identify a phase model, both experimentally and from high-dimensional neuron models, one may utilise the concept of the (linear) phase-response curve (PRC). Theoretical derivations of PRCs for perturbations along the dynamics in the centre-manifold of several onset bifurcations in neuronal systems have been discussed[26–28]. Here, this approach is extended to perturbations of the gating kinetics (see *Conjecture 7*) and – for the first time – the contributions of perturbations in all dimensions are derived. Furthermore, we demonstrate that for different spike-onset bifurcations such as the SNIC or small- and big-SNL bifurcations, the tangent space to the isochrones near the ghost of the saddle-node (SN) is given by the strongly-stable eigenvectors of the Jacobian at the saddle-node (see *Conjecture 6*).

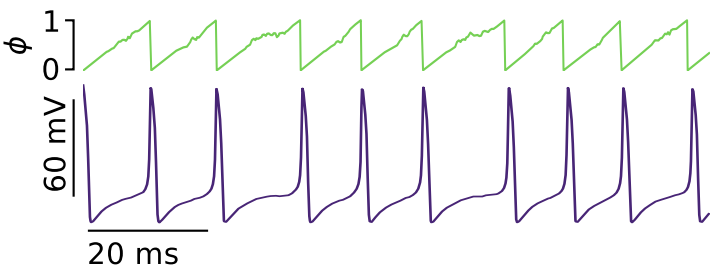

Fig. 1

The phase equation turns the spiking neuron into a one-dimensional level-crossing process with equivalent spike times. The phase is plotted modulo 1.

Spike-onset bifurcations

With an increase of $I_{\rm in}$ there are a number of possible onset bifurcations (or bifurcation sequences) that can lead from resting states to a tonic spiking regimes in neurons[29]. Among them are sub- and supercritical Hopf bifurcations as well as different types of homoclinic orbits emerging from a saddle-node. Desideratum (iii) rules out supercritical Hopf bifurcations due to the fact that their invariant cycles (or spikes) follow a square-root amplitude scaling at creation and thus violate the all-or-none principle. A subcritical Hopf bifurcation followed by a fold of invariant cycles is ruled out by desiderata (ii) and (iv), since they start with a finite firing rate and a region of bistability. Desideratum (iv), furthermore, rules out that spiking emerges from a homoclinic-orbit to a saddle, which also shows bistability. Consequently, this article focuses on invariant cycles that emerge from homoclinic-orbits to a saddle-node. Several configurations are possible depending on which approach the orbit takes upon converging back to the saddle-node, see *Fig. 2*. One such bifurcation, the codimension-1 *saddle-node on invariant cycle* (SNIC) ranks prominently as the onset of spiking in many neuronal models[14,26,30]. Introducing a second parameter that controls the time scale separation between voltage and kinetic equations in Eq. (1), it was conjectured (and shown for planer systems) that this SNIC bifurcation is always enclosed by two codimension-2 saddle-node loop bifurcations[31]. They result in a small- and big-homoclinic loop. Further consequences of this transition are discussed in the following.

Def. 2 *(A sequence of spike-onset bifurcations)*

The following three different spike-onset bifurcations comply with *Assumptions # (i-iv)*. Formally, it is assumed that the neuron model has a structurally unstable equilibrium (saddle-node equilibrium) at $\vec{x}_{\rm sn}$ with Lyapunov exponents $\Re\lambda_0 = 0$ and $\Re\lambda_i < 0$ for $i > 0$. Furthermore, the stable and unstable manifolds of the saddle-node equilibrium are globally connected, such that they form transverse homoclinic orbits. From those, the invariant cycles that constitute tonic spiking emerge when the saddle-node vanishes in a codimension-1 bifurcation. There are three important possibilities for the homoclinic connections, illustrated in *Fig. 2*:

Big saddle node loop (big-SNL): In this case, the loop leaves the saddle-node via the semi-stable manifold and enters via the strongly stable manifold in the direction that causes the loop to encircle all three former fixpoints of the neuron model, *cf. Fig. 2a*.

Saddle-node on invariant cycle (SNIC): In this case the homoclinic orbit leaves via the semi-stable manifold and returns via the semi-stable manifold, *cf. Fig. 2b*.

Small saddle node loop (small-SNL): In this case, the loop leaves the saddle-node via the semi-stable manifold and enters via the strongly stable manifold but encircles only one fixpoint of the neuron model, *cf. Fig. 2*.

General properties of the codimension-2 bifurcation that flips between SNIC and big-SNL and SNIC and small-SNL have been discussed[32].

For neuron models, it was shown previously that increasing the relative time scale between the current-balance equation and the gating kinetics, the following sequence of bifurcations is traversed: big-SNL $\rightarrow$ SNIC $\rightarrow$ small-SNL[31]. For example, increasing the membrane capacitance, $C_{\rm m}$, can induce this sequence, such that the interval of capacitance values that give rise to a SNIC bifurcation is encapsulated by the two SNL points, $C_{\rm m}^{\text{big-SNL}} < C_{\rm m}^{\rm SNIC} < C_{\rm m}^{\text{small-SNL}}$.

In order to induce such a flip bifurcation, an infinitesimal parameter perturbation that affects the time-scale difference between gating kinetics and membrane time constant is sufficient. The flips switch the approach to the saddle-node from the semi-stable manifold to the strongly-stable manifold, leaving the departure unaltered[33]. This breaks the symmetry of the dynamics in the centre-manifold as well as the PRC and has stark consequences for neuronal dynamics and coding[31].

The big-SNL bifurcations switch the SNIC (*Fig. 2*b) to the big homoclinic loop (*Fig. 2*a), while the small-SNL bifurcation flips the SNIC to the small homoclinic loop (*Fig. 2*c).

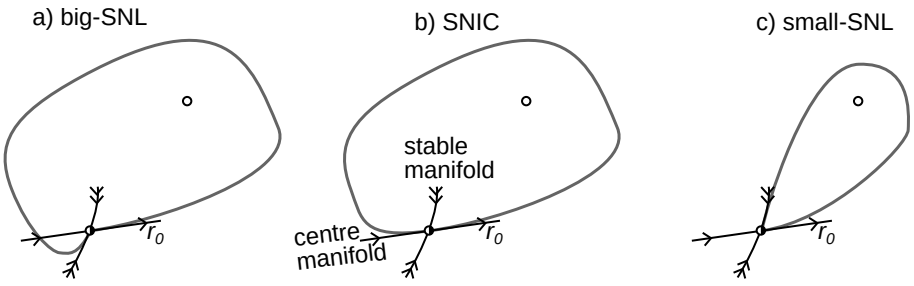

Fig. 2

Illustrations of the centre-manifold and homoclinic orbits at the SNIC bifurcation and small- and big-SNL points in a planar Na^+-K^+ neuron model.

Isochrones and phase-response curves

In order to study the properties of isochrones and phase dynamics near saddle-node loop bifurcations in the next section, we now review some basic definitions and properties regarding the phase dynamics. Let us first define the phase-response curve (PRC) of a neuronal oscillator.

Def. 3 *(Phase response curve)*

The *phase gradient* w.r.t. the state variables, $\vec{\nabla}\psi$, from Eq. (4) is also called *phase response curve* (PRC). The PRC of a self-sustained limit-cycle oscillator with a neutral direction given by the zero-Floquet exponent, is a periodic vector-valued function, $\vec{\nabla}\psi(\phi) : I\!R \to I\!R^n$. It yields the linear phase-response in the sense that infinitesimally short perturbations $\Delta\vec{x}$ projected onto it at a given phase $\phi \in \mathbb{R}$ are mapped to *constant* shifts in phase

$$\Delta\psi = \vec{\nabla}\psi(\phi) \cdot \Delta\vec{x}(\phi) = \text{const.}$$

Remark 1

If controlled perturbations are feasible, the PRC is an experimentally accessible quantity[25] in addition to being a well defined mathematical concept. Note that this is exactly the definition required to experimentally measure PRCs: apply short pulses and compare perturbed and unperturbed periods. In fact, the constancy of the phase shift is a prerequisite for it to be measurable.

The phase-response curves for perturbations along the semi-stable manifold of SNIC and SNL bifurcations are known, yet to map out perturbations in all the gating dimensions, they need to be extended to the full state space.

For an initial condition $\vec{y} \in I\!R^n$, the model in Eq. (2) generates a flow $\vec{x}(t;\vec{y}) : I\!R^+ \times I\!R^n \to I\!R^n$. A stable invariant cycle was demanded in *Assumption* #(i) and w.o.l.o.g. one may assume $\vec{x}_{\rm ic}(0)$ to be at the voltage maximum of the spike. Denote the invariant cycle as $\Gamma = \{\vec{x}(t;\vec{x}_{\rm ic}(0)) : 0 \leqslant t < T_{\rm p}\}$, which has a basin of attraction, $\mathcal{B}$, such that $\forall\vec{y} \in \mathcal{B} : \lim_{k\to\infty} \vec{x}(kT_{\rm p};\vec{y}) \in \Gamma$. The associated Floquet exponents, ν_k, of Γ are negative except for the one neutral dimension, so that they can be ordered as

$$0 = \nu_0 > \nu_1 \geqslant ... \geqslant \nu_{n-1}. \quad (5)$$

Each element of the invariant cycle's basin of attraction can be associated with an asymptotic phase.

Def. 4 *(Assymptotic phase)*

Denote the flow of the dynamical system in Eq. (2) that conforms with *Assumption* # and with initial condition $\vec{y}$ as $\vec{x}(t;\vec{y})$. The asymptotic phase, ψ, of a point in the basin of attraction, $\vec{y} \in \mathcal{B}$, is

$$\psi(\vec{y}) = \text{argmin}_{\psi} \lim_{t\to\infty} \|\vec{x}(t;\vec{y}) - \vec{x}_{\rm ic}(t + \psi T_{\rm p})\|. \quad (6)$$

Based on the asymptotic phase, the concept of isochrons can be introduced[34,35].

Def. 5 *(Isochrons)*

The *isochron* manifolds, $\mathcal{I}(\phi)$, are the level sets of the asymptotic phase variable

$\mathcal{I}(\phi) = \{\vec{y} \in \mathcal{B} : \psi(\vec{y}) = \phi\}$.

*Fig. 3*a-c shows the isochrons at equidistant phases for the three bifurcation types considered in this article. The limit cycles (dashed) are close to the homoclinic orbits of the saddle. One observes a high isochron density near the saddle.

Next, denote the Jacobian of Eq. (2)'s flow-field as, $\boldsymbol{J}(\vec{x}) = \vec{\nabla} \otimes \vec{F}(\vec{x})$. For an arbitrary point in state space, the Jacobian has the following eigensystem

$$\vec{l}_k\boldsymbol{J} = \lambda_k\vec{l}_k \text{ and } \boldsymbol{J}\vec{r}_k = \lambda_k\vec{r}_k, \text{ with } \vec{l}_k \cdot \vec{r}_j = \delta_{kj}. \quad (7)$$

Here, the system is typically examined at the saddle-node where the eigenvalues can be ordered as

$0 = \lambda_0 > \lambda_1 \geqslant ... \geqslant \lambda_{n-1}$.

Furthermore, if $\vec{x} \in \Gamma$, the Jacobian can be addressed as a function of the phase. Hence one may shorten $\boldsymbol{J}(\phi) = \boldsymbol{J}(\vec{x}_{\rm ic}(T_{\rm p}\phi))$. This gives rise to the $T_{\rm p}$-periodic linear matrix equation studied in Floquet theory to analyse the stability of invariant cycles.

Def. 6 *(Floquet modes)*

The *Floquet modes*, $W_k(\phi)$ corresponding to a Floquet exponent ν_k, are the periodic solution to the first variational system on the invariant cycle

(8) $\frac{\mathrm{d}}{\mathrm{d}\phi}\vec{W}_k(\phi) = (\boldsymbol{J}(\phi) - \nu_k \boldsymbol{I})\vec{W}_k(\phi)$, s.t. $\vec{W}_k(0) = \vec{W}_k(1)$.

The *adjoint Floquet modes* are the periodic solutions to

(9) $\frac{\mathrm{d}}{\mathrm{d}\phi}\vec{Z}_k(\phi) = \vec{Z}_k(\phi) \cdot (\nu_k \boldsymbol{I} - \boldsymbol{J}(\phi))$, s.t. $\vec{Z}_k(0) = \vec{Z}_k(1)$,

with $\forall \phi : \vec{Z}_j(\phi) \cdot \vec{W}_k(\phi) = \delta_{jk}$.

The solutions to Eq. (8) and (9) are 1-periodic non-trivial functions. They have at least one maximum and minimum on $\phi \in [0, 1]$. It turns out that the phase-response curve adhering to *Def. 3* corresponds to the zeroth adjoint Floquet mode.

Observation 1 *(Adjoint equation)*

The phase-response curve, as defined in *Def. 3*, is equivalent to the zeroth adjoint Floquet mode ($k = 0$ in Eq. (9)), *i.e.*, for $\nu_0 = 0$ it follows $\vec{Z}_0(\phi) = \vec{\nabla}\psi(\phi)$. This means

(10) $\frac{\mathrm{d}}{\mathrm{d}\phi}\vec{Z}_0(\phi) = -\vec{Z}_0(\phi) \cdot \boldsymbol{J}(\phi)$.

Proof 1

Def. 3 demands that there be a constant phase shift $\Delta\psi$ after some perturbation. With the definition of the phase in Eq (6), *Def. 4*, the phase shift to lowest order is $\Delta\psi = (\frac{\partial\psi}{\partial\vec{x}_{\mathrm{ic}}} \cdot \Delta\vec{x})$. Denote $\vec{Z}(t) = \frac{\partial\psi}{\partial\vec{x}_{\mathrm{ic}}}$ and $\vec{y} = \Delta\vec{x}$. Small changes in the dynamics evolve as $\dot{\vec{y}} = \boldsymbol{J}(\vec{x}_{\mathrm{ic}}(t))\vec{y}$. Then, from $\frac{\mathrm{d}\Delta\psi}{\mathrm{d}t} = 0$, it follows

$0 = (\frac{\mathrm{d}}{\mathrm{d}t}\vec{Z}(t) \cdot \vec{y}(t)) + (\vec{Z}(t) \cdot \frac{\mathrm{d}}{\mathrm{d}t}\vec{y}(t)) = (\frac{\mathrm{d}}{\mathrm{d}t}\vec{Z}(t) \cdot \vec{y}(t)) + (\vec{Z}(t) \cdot \boldsymbol{J}(t)\vec{y}(t)) = (\frac{\mathrm{d}}{\mathrm{d}t}\vec{Z}(t) \cdot \vec{y}(t)) + (\vec{Z}(t)\boldsymbol{J}(t) \cdot \vec{y}(t))$.

Since $y(t)$ is arbitrarily non-zero, the Fredholm alternative requires $\frac{\mathrm{d}}{\mathrm{d}t}\vec{Z}(t) + \vec{Z}(t)\boldsymbol{J}(t) = 0$. Substituting $t = T_{\mathrm{p}}\phi$, one recovers Eq. (10).

Eq. (10) has been previously derived[28]. Here we identify it with the zeroth Floquet mode, which is part of the orthonormal system of Eqs. (8) and (9). Recall the definition of the gradient as the normal to the level set. Then, as a consequence, *Observation 1* implies that the tangent space to the isochrons is spanned by the rest of the orthonormal system in Eq. (8). This relation has been previously used by 36.

Corollary 2 *(Tangent space of the isochrons)*

The tangent space of the isochrons at the point where they cross the invariant cycle, $\mathcal{T}_{\vec{x}_{\mathrm{ic}}}\mathcal{I}$, is spanned by the non-zero Floquet modes

$\mathcal{T}_{\vec{x}_{\mathrm{ic}}}\mathcal{I}(\phi) = \left\{\sum_k a_k W_k(\phi) : k > 0, a_k \in I\!R\right\}$.

From *Def. 6* and *Observation 1* and *Corollary 2* it follows that the PRC is the normal to the tangent space of the isochrons

(11) $\vec{Z}_0(\phi) \in \mathcal{T}_{\vec{x}_{\mathrm{ic}}}\mathcal{I}(\phi)^{\perp}$.

The phase response curve is a bounded 1-periodic vector-valued function which according to the mean value theorem has at least one maximum and minimum. Next follows a rather simple relation between isochrons and PRCs. Consequences for the change in isochrons and PRC shape at the bifurcations (mentioned in *Def. 2*) are examined later. In general, the following relation between the PRC vector and the tangent space to the isochrons holds:

Observation 3 *(Tangent space and PRC extrema)*

Assume that $\vec{Z}_0$ has a left and or right derivative at ϕ_{ex}. If and only if the phase-response curve, $\vec{Z}_0(\phi)$, has an extremum in each dimension at ϕ_{ex}, such that $\frac{\mathrm{d}}{\mathrm{d}\phi}\vec{Z}_0(\phi)|_{\phi=\phi_{\mathrm{ex}}} = \vec{0}$, then the tangent space of the isochrons at this point is spanned by the stable eigenvectors (all besides $\vec{r}_0$) of the Jacobian, $\boldsymbol{J}(\phi_{\mathrm{ex}})$, *i.e.*,

$\mathcal{T}_{\vec{x}_{\mathrm{ic}}}\mathcal{I}(\phi_{\mathrm{ex}}) = \left\{\sum_{k=1}^{n-1} a_k\vec{r}_k : \boldsymbol{J}(\phi_{\mathrm{ex}})\vec{r}_k = \lambda_k\vec{r}_k, \lambda_k < 0\right\}$.

Proof 3 If the PRC at the extremum is nontrivial, $\vec{Z}_0(\phi_{\mathrm{ex}}) \neq 0$, then due to the left-right orthonormality, all other (adjoint) Floquet modes also have vanishing derivatives. $\vec{W}_j'(\phi_{\mathrm{ex}}) = \vec{Z}_k'(\phi_{\mathrm{ex}}) = 0$ in Eqs. (8) and (9) yields $(\boldsymbol{J}(\phi_{\mathrm{ex}}) - \nu_j)\vec{W}_j(\phi_{\mathrm{ex}}) = 0$ and $\vec{Z}_k(\phi_{\mathrm{ex}}) \cdot (\boldsymbol{J}(\phi_{\mathrm{ex}}) - \nu_k) = 0$. Consequently, $\nu_j, \vec{Z}_j(\phi_{\mathrm{ex}}), \vec{W}_j(\phi_{\mathrm{ex}})$ form the left-right eigensystem of the Jacobian and the Floquet exponents equal the Lyapunov exponents at this point.

In which regime does a neuron model have a phase value at which all the PRC components' derivatives vanish in all dimensions simultaneously, and what phase would that be? As is shown in the next section, this happens, *e.g.*, if the dynamics is close to the centre-manifold of the onset-bifurcations in *Def. 2*.

Phase-response curves at SNIC and SNL bifurcations

One-dimensional ODEs with reset have been used as heuristic neuron models[37]. A clear relationship between conductance-based neuron models and the quadratic integrate-and-fire model was forged by projecting the dynamics onto the centre-manifold of the SNIC bifurcation[26,30].

Observation 4 *(PRCs in the centre-manifold of SNIC and SNL)*

With *Assumption #* (ii), that the period of the invariant cycle is large compared to all time scales of the system, the PRCs for perturbations along the semi-stable manifold of SNIC and the small- and big-SNL bifurcations are

(12) $Z^{\rm snic}_{\rm cm}(\phi) = \frac{T^{\rm snic}_{\rm p} b}{2\pi^2}(1-\cos(2\pi\phi))$ and $Z^{\rm snl}_{\rm cm}(\phi) = \frac{2T^{\rm snl}_{\rm p} b}{\pi^2}(1+\cos(\pi\phi))$,

respectively. The constant is given by

$b = \vec{l}_0^{\rm sn}\boldsymbol{H}(\phi_{\rm sn})\vec{r}_0^{\rm sn}\vec{r}_0^{\rm sn}$, where $\boldsymbol{H}$ is the Hessian tensor of the flowfield, $\boldsymbol{H} = \vec{\nabla}\otimes\vec{\nabla}\otimes\vec{F}$.

The period scaling is $T^{\rm snl}_{\rm p} = \frac{\pi}{2\sqrt{ab}}$ and $T^{\rm snic}_{\rm p} = \frac{\pi}{\sqrt{ab}}$, respectively.

For $T_{\rm p}\to\infty$, the maxima are located at the phase which corresponds to the point where the dynamics passes the saddle-node, at $\phi_{\rm sn} = {\rm argmax}_\phi\, Z(\phi)$. This is at

(13) $$\lim_{T_{\rm p}\to\infty}\phi_{\rm sn} = \begin{cases}\frac{1}{2} & : \text{SNIC},\\ 0 & : \text{SNL}.\end{cases}$$

At the respective $\phi_{\rm sn}$, the derivative of the PRC vanishes, that is

(14) $\lim_{\phi\searrow 0}\frac{\rm d}{{\rm d}\phi}Z^{\rm snl}_{\rm cm}(\phi) = 0$ and $\frac{\rm d}{{\rm d}\phi}Z^{\rm snic}_{\rm cm}(\phi)|_{\phi=\frac{1}{2}} = 0$.

Proof 4

For $I_{\rm in}\to I_{\rm sn}$, and hence $T_{\rm p}\to\infty$, the dynamics is confined to the tangent of the semi-stable manifold, $\vec{r}_0$, for arbitrarily long portions of the period. The first part of the derivation follows a previous calculations[26]. Consider the dynamics near the saddle-node $\vec{x}_{\rm sn}$. Define $\vec{w}(t) = \vec{x}(t) - \vec{x}_{\rm sn}$. The saddle-node exists at a particular parameter value $I_{\rm sn}$, such that $\frac{\rm d}{{\rm d}t}\vec{x}_{\rm sn} = \vec{F}(\vec{x}_{\rm sn}; I_{\rm sn}) = 0$, where the parameter dependence was made explicit. The structure of Eq. (1) allows one to split the vector field into $\vec{F}(\vec{x}; I_{\rm in}) = \vec{F}(\vec{x}; I_{\rm sn}) + \vec{G}(\vec{x}; I_{\rm in} - I_{\rm sn})$, where

$\vec{G} = [(I_{\rm in}-I_{\rm sn})/C_{\rm m}, 0, ..., 0]^\top$.

Expanding the vector field to second order around $\vec{x}_{\rm sn}$, the dynamics can be written as

$\frac{\rm d}{{\rm d}t}\vec{w} = \vec{G}(\vec{x}_{\rm sn}; I_{\rm in}-I_{\rm sn}) + \boldsymbol{J}(\vec{x}_{\rm sn})\vec{w} + \boldsymbol{H}(\vec{x}_{\rm sn})\vec{w}\vec{w}$.

Expressing the dynamics along the centre-manifold as $\vec{w}(t) = y(t)\vec{r}_0^{\rm sn}$, one may project onto the left eigenvector of the Jacobian at the saddle-node, $\vec{l}_0^{\rm sn}\boldsymbol{J}(\vec{x}_{\rm sn}) = \vec{0}$, and obtain an equation for the coefficient along the centre-manifold

(15) $\dot{y} = a + by^2$, with $a = \vec{l}^{\rm sn}_{00}(I_{\rm in}-I_{\rm sn})/C_{\rm m}$ and b as in the theorem.

Now $y\in K\subset\mathbb{R}$ indicates the position of the dynamics on the slow semi-stable manifold. At the SNIC, $K=(-\infty,\infty)$. In the SNL case, $K=[0,\infty)$. The slowest dynamics, and therefore the highest isochron density, is closest to the former saddle-node, at $y(t^{\rm sn}) = 0$. The solution for arbitrary initial condition $y(0)$ is

(16) $y(t) = \sqrt{\frac{a}{b}}\tan\left(\sqrt{ab}\,t+\theta\right)$, where $\theta = \arctan\left(y(0)\sqrt{b/a}\right)$.

The solution diverges, just as a spike would, $\lim_{t\to\infty}y(t) = \infty$. However, for a given initial condition, $y(0)$, the time until $y(T_{\rm p}) = \infty$ is finite. Its reciprocal is the neuron's firing rate, $f_0 = 1/T_{\rm p}$. The period is given by

(17) $T_{\rm p} = \frac{\pi/2-\theta}{\sqrt{ab}}$, *i.a.*, $T^{\rm snl}_{\rm p} = \frac{\pi}{2\sqrt{ab}}$ and $T^{\rm snic}_{\rm p} = \frac{\pi}{\sqrt{ab}}$.

Depending on the initial conditions

(18) $$t^{\rm sn} = \begin{cases}0 & : y(0) = 0,\\ T_{\rm p}/2 & : y(0) = -\infty.\end{cases}$$

The PRC is defined as the phase gradient w.r.t. the state variables[19,36]. PRCs of simple 1D reset-models, such as the quadratic equation of Eq. (15), can be calculated as the reciprocal of the vector field on the solution. The PRC is

$Z_{\rm cm}(\phi) = \frac{\partial\phi}{\partial y} = \dot{\phi}\frac{\partial t}{\partial y} = \frac{f_0}{\dot{y}} = \frac{f_0}{a+by^2(T_{\rm p}\phi)}$.

Here, the fact was used that in the unperturbed case the phase progresses as $\dot{\phi} = f_0$. Inserting the solution of Eq. (16) yields

$Z_{\rm cm}(\phi) = \frac{f_0}{a+a\tan^2((\pi/2-\theta)\phi+\theta)} = \frac{f_0}{a}\cos^2((\pi/2-\theta)\phi+\theta) = \frac{bT_{\rm p}}{2(\pi/2-\theta)^2}(1+\cos((\pi-2\theta)\phi+2\theta))$.

Note that a depends on the bifurcation parameter, yet b does not. Hence, it may be preferable to have a scaling with the bifurcation parameter via the firing rate only. For the two cases $\theta = -\frac{\pi}{2}$ and $\theta = 0$ corresponding to SNIC and SNL bifurcation, respectively, one recovers the identities in Eq. (12). From Eq. (18) we obtain $\phi_{\rm sn}$ in Eq. (13) at the two bifurcations. The derivatives of $Z^{\rm snic}_{\rm cm}(\phi)$ and $Z^{\rm snl}_{\rm cm}(\phi)$ vanish at $\phi = \frac{1}{2}$ and $\phi = 0$, respectively.

Remark 2

The vanishing derivative does not occur at a homoclinic-orbit to a saddle (beyond the SNL bifurcation). Although the canonical PRC for a homoclinic to a saddle has been reported to have a peak[28], its derivative at the maximum was argued to be nonzero due to a discontinuity.

The general PRC shapes are exemplified in *Fig. 4* for the Traub-Miles neuron model[38] for which the boundary value problem in Eq. (10) was solved numerically. One may confirm the symmetric PRC at the SNIC onset-bifurcation (*Fig. 4a*) and the asymmetric PRC at the small-SNL point (*Fig. 4b*). Some implications of this symmetry breaking have been discussed previously[31]. With the general shape and properties of the PRCs in the centre-manifold of the SNIC and SNL bifurcations established by *Observation 4*, we now turn to the case where perturbations are given along the different gating dimensions. In other words, one needs to establish the contributions of the different kinetic gates and the voltage dimension to the centre-manifold. Due to the particular structure of conductance-based neuron models in *Def. 1*, the required eigensystem can be solved analytically:

Observation 5 *(Eigensystem of a conductance-based neuron model at the sadde-node)*

Consider a conductance-based neuron model (*Def. 1*) at a SNIC or SNL bifurcation (*Assumption 2*), *i.e.*, with a simple zero eigenvalue, $\lambda_0 = 0$, at the saddle-node. Then the semi-stable (centre-)manifold is tangential to the right eigenvector corresponding to λ_0, which is given by

$$(19)\quad \vec{r}_0^{\,\mathrm{sn}} = \tfrac{1}{\kappa}\begin{pmatrix} 1 \\ \tau_k \frac{\partial F_k}{\partial v} \\ \vdots \end{pmatrix} = \tfrac{1}{\kappa}\begin{pmatrix} 1 \\ \frac{\mathrm{d}}{\mathrm{d}v} a_k^{(\infty)}(v)|_{v=v_{\mathrm{sn}}} \\ \vdots \end{pmatrix},$$

where $v = v_{\mathrm{sn}}$ and $a_k = a_k^{(\infty)}(v_{\mathrm{sn}})$ was used. The normalisation constant κ is given at the end of *Proof 5*.

The associated left eigenvector is

$$(20)\quad \vec{l}_0^{\,\mathrm{sn}} = \begin{pmatrix} 1 \\ \tau_k \frac{\partial F_0}{\partial a_k} \\ \vdots \end{pmatrix},$$

where F_0 denotes the r.h.s. of the current-balance equation and F_k for $k = 1, ..., n-1$ the r.h.s. of the kinetic equations. Note that the right eigenvector $\vec{r}_0$ gives the direction of the semi-stable manifold.

Proof 5

The special structure of the Jacobian in a conductance-based neuron model, a rank-1 updated diagonal matrix,

$$\boldsymbol{J} = \begin{pmatrix} \frac{\partial F_0}{\partial v} & \frac{\partial F_0}{\partial a_1} & \cdots & \frac{\partial F_0}{\partial a_{n-1}} \\ \frac{\partial F_1}{\partial v} & \frac{\partial F_1}{\partial a_1} & & 0 \\ \vdots & & \ddots & \\ \frac{\partial F_{n-1}}{\partial v} & 0 & & \frac{\partial F_{n-1}}{\partial a_{n-1}} \end{pmatrix},$$

allows for an explicit calculation of the left and right eigenvectors corresponding to the eigenvalue $\lambda_0 = 0$.

Choosing the zero eigenvector as $\vec{r}_0 = \binom{1}{\vec{\mu}}$, one obtains from $\boldsymbol{J}\vec{r}_0^{\,\mathrm{sn}} = \lambda_0 \vec{r}_0^{\,\mathrm{sn}} = 0$ a set of n equations:

(21) $\frac{\partial F_0}{\partial v} + \sum_{j=1}^{n-1} \mu_j \frac{\partial F_0}{\partial a_j} = 0$, and

(22) $\frac{\partial F_k}{\partial v} + \mu_k \frac{\partial F_k}{\partial a_k} = 0$ for $k = 1, ..., n-1$.

From Eqs. (22), it follows that $\mu_j = -\left(\frac{\partial F_j}{\partial a_j}\right)^{-1} \frac{\partial F_j}{\partial v}$. This solution also solves Eq. (21), because the required zero eigenvalue implies that $\det \boldsymbol{J} = 0$. Note that according to Leibniz's formula the determinant of $\boldsymbol{J}$ is

$$(23)\quad \det \boldsymbol{J} = \left| \frac{\partial F_0}{\partial v} - \sum_{j=1}^{n-1} \left(\frac{\partial F_j}{\partial a_j}\right)^{-1} \frac{\partial F_j}{\partial v} \frac{\partial F_0}{\partial a_j} \right| \prod_{k=1}^{n-1} \frac{\partial F_k}{\partial a_k} = 0.$$

Since $\frac{\partial F_k}{\partial a_k} = -\frac{1}{\tau_k(v_{\mathrm{sn}})} < 0$, the first factor of the determinant must be zero. Hence, μ_j also solves Eq. (21).

An analogue derivation for the left eigenvector, $\vec{l}_0 = \binom{1}{\vec{\xi}}$, results in the following set of equations,

(24) $\frac{\partial F_0}{\partial v} + \sum_{j=1}^{n-1} \xi_j \frac{\partial F_j}{\partial v} = 0$, and

(25) $\frac{\partial F_0}{\partial a_k} + \xi_k \frac{\partial F_k}{\partial a_k} = 0$ for $k = 1, ..., n-1$,

which yields $\xi_j = -\left(\frac{\partial F_j}{\partial a_j}\right)^{-1} \frac{\partial F_0}{\partial a_j}$. The normalisation constant to ensure $\vec{l}_0^{\,\mathrm{sn}} \cdot \vec{r}_0^{\,\mathrm{sn}} = 1$ is

$\kappa = 1 + \sum_{j=1}^{n-1} \tau_j^2 \frac{\partial F_0}{\partial a_j} \frac{\partial F_j}{\partial v}\Big|_{v=v_{\mathrm{sn}}, a_k = a_k^{(\infty)}(v_{\mathrm{sn}})}$. Note that y is in units of volt here. Other conventions are possible.

The derivation builds on results from by 39, where the system of generalized eigenvectors was derived for a conductance-based neuron model at a Bogdanov-Takens cusp point. The analytical expression for the left and right eigenvectors to the zero eigenvalue stated here are in principle independent of whether there is a homoclinic orbit attached to the saddle-node or not.

Due to the particular form of Eq. (19), one can state the following observation about the contributions of different gating dimensions to the centre-manifold:

Remark 3 *(Centre-manifold contributions from all gates)*

Physiologically plausible conductance-based neuron models typically show strictly monotonous (sigmoidal) activation functions $a_k^{(\infty)}(v)$, *i.e.* $\forall v : \frac{\mathrm{d}}{\mathrm{d}v} a_k^{(\infty)}(v) \neq 0$. The maximum slope is usually at the voltage at which half of the channels are open (their *activation threshold*). In that case, the semi-stable (centre-)manifold in Eq. (19) has contributions from the directions of all gating variables and thus is not parallel to the voltage direction. For example, the coefficients of $\vec{r}_0^{\,\mathrm{sn}}$, corresponding to gates of some ion channels – like the delayed-rectifying K^+ channel with higher threshold – may be small in magnitude at the rheobase, while the direction of the low-threshold Na^+ channels may be more significant.

As a consequence of *Remark 3*, the tangent vector to the centre-manifold has contributions from all dimensions, and all gating dynamics follow the same quadratic dynamics near the saddle-node with the same consequence for perturbations and PRCs:

Remark 4 *(PRC shape of gating kinetics)*

For an invariant cycle originating from a homoclinic orbit to a saddle-node, where the departing dynamics from the SN is governed by the quadratic dynamics of the centre-manifold, the PRC shape is the same in all state variables. *Inter alia*, the extrema of the PRC are located at the same phase in all dimensions,
$\frac{\mathrm{d}}{\mathrm{d}\phi}\vec{Z}(\phi_{\mathrm{sn}}) = \vec{0}$.
Indeed, it is clear that this is the maximum of the PRC, since the isochron density is highest when the dynamics is slow, as is the case near the centre-manifold of the saddle-node.

Hence, *Remark 4* ensures that the conditions for *Observation 3* are met near the saddle-node, in particular near the onset of firing via the SNIC ans SNL bifurcations.

Remark 5

Note that invariant cycles that emerge via a supercritical Hopf bifurcation or the Bautin bifurcation (subcritical Hopf followed by a fold of invariant cycles) by the mean value theorem must have vanishing derivatives of the PRC in each dimension, but not in all dimension at once. This is already the case for the PRCs in their two-dimensional centre-manifold[28]. Hence *Observation 3* is not applicable.

Conjecture 6 *(Isochron structure at the saddle-node)*

For neuron models near SNIC and small/big-SNL onset bifurcations, the dynamics near the saddle-node shows the highest isochron density. For homoclinic orbits attached to a saddle-node, the tangent plain to the isochrons at the saddle is spanned by the stable manifolds of the saddle, *i.e.*

(26) $\boldsymbol{J}(\phi_{\mathrm{sn}})\vec{W}_k(\phi_{\mathrm{sn}}) = \lambda_k \vec{W}_k(\phi_{\mathrm{sn}})$.

Hence, $\vec{W}_k(\phi_{\mathrm{sn}})$ is an eigenvector to the Jacobian. The tangent space to the isochrons, Eq. (11), at ϕ_{sn} is

(27) $\mathcal{T}_{\vec{x}_{\mathrm{ic}}(\phi_{\mathrm{sn}})}\mathcal{I}(\phi_{\mathrm{sn}}) = \{\vec{r}_k : \boldsymbol{J}(\phi_{\mathrm{sn}})\vec{r}_k = \lambda_k \vec{r}_k, \lambda_k < 0\}$.

The PRC lies in the orthogonal complement of the tangent space $\vec{Z}(\phi_{\mathrm{sn}}) \in \mathcal{T}_{\vec{x}_{\mathrm{ic}}}\mathcal{I}(\phi)^{\perp}$, and thus points into the same direction as $\vec{l}_0$.

Proof 6

In the limit $T_{\mathrm{p}} \to \infty$ the isochron density becomes arbitrarily high near the saddle-node. Hence, in line with *Observation 4*, the phase susceptibility in this region will be maximal, *i.e.*, $\phi_{\mathrm{sn}} = \phi_{\mathrm{ex}}$. Hence, $\vec{Z}_0'(\phi_{\mathrm{sn}}) = 0$, and Eqs. (26) and (27) follow immediately from *Observation 3*.

The isochron structure at the saddle-node was mentioned by 28 without proof.

Examples for the isochrons of the three onset bifurcations can be inspected in *Fig. 3*. Note that the isochrons are almost tangential to the invariant cycle close to the strongly stable manifold of the saddle in *Fig. 3*a and *Fig. 3*b. Isochrons are the foliations of tangent bundles of phaseless sets[35]. Beyond the small-SNL bifurcation saddle and node detach. Therefore, the invariant cycle then emerges from the homoclinic orbit to the saddle. In this case, the system gets bistable and the strongly stable manifold acts as a separatrix on the other side of which there is a stable node. All isochrons are foliations of the tangent bundle of this separatrix. Beyond the big-SNL, the system also becomes bistable, but in this case the stable node resides inside the limit cycle and the separatrix bends around it.

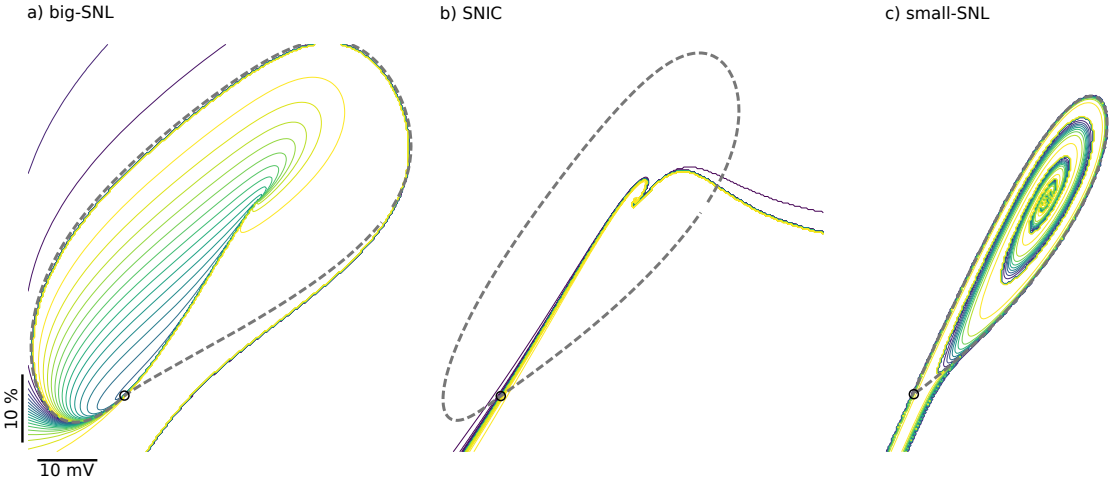

Fig 3

Isochrons of big-SNL point (a), SNIC bifurcation (b) and small-SNL point (c) in a 2D Na^+-K^+ neuron model[29]. Shown is the K^+ channel open probability *vs.* the membrane voltage. Dashed lines depict the invariant orbit close to the homoclinic orbit.

Conjecture 6 states that the PRC vector at the saddle-node points into the direction of $\vec{l}_0^{\,\mathrm{sn}}$. We also know that the saddle-node has the (nonzero) maximum of the PRC (*Observation 4*) and that the PRC shape is the same in all dimensions (*Remark 4*). Therefore, the correct relative scaling of the PRC for all phases is given by $\vec{l}_0^{\,\mathrm{sn}}$, for which the analytical expression is given by Eq. (20) in *Observation 5*.

Conjecture 7 *(Relative weighting of the phase-response vector)*

The infinitesimal phase-response curve of an invariant cycle originating from a homoclinic orbit at a saddle-node is given by

$\vec{Z}_{\mathrm{sn}}^{\mathrm{hom}}(\phi) = \vec{l}_0^{\,\mathrm{sn}} Z_{\mathrm{cm}}(\phi)$,

where Z_{cm} is stated in *Observation 4* and $\vec{l}^{\,\mathrm{sn}}$ in *Observation 5*.

Proof 7

This follows directly from a projection of $\vec{Z}_{\mathrm{sn}}^{\mathrm{hom}}$ on the centre-manifold, $\vec{r}_0^{\,\mathrm{sn}} \cdot \vec{Z}_{\mathrm{sn}}^{\mathrm{hom}} = Z_{\mathrm{cm}}$, and the normalisation $\vec{l}_0^{\,\mathrm{sn}} \cdot \vec{r}_0^{\,\mathrm{sn}} = 1$.

Making use of the expression in *Observation 4*, one can state the complete PRC vector.

Corollary 8 *(Full phase response of SNIC and SNL neuron models)*

The vector of phase-response curves, $\vec{Z}_0(\phi)$, with the phase susceptibilities of all kinetic gating equations of a conductance-based neuron model described in Eq. (2), near the semi-stable manifold of a SNIC and an SNL bifurcation is given by

$\vec{Z}_0^{\mathrm{snic}}(\phi) = \vec{l}_0^{\,\mathrm{sn}} \frac{T_{\mathrm{p}}^{\mathrm{snic}} b}{2\pi^2}(1-\cos(2\pi\phi))$ and $\vec{Z}_0^{\mathrm{snl}}(\phi) = \vec{l}_0^{\,\mathrm{sn}} \frac{2T_{\mathrm{p}}^{\mathrm{snl}} b}{\pi^2}(1+\cos(\pi\phi))$, respectively.

Here, $\vec{l}_0^{\,\mathrm{sn}}$ is the left eigenvector to the Jacobian at the saddle. It is normal to the tangent space of the isochrons and is given by

$$\vec{l}_0^{\,\mathrm{sn}} = \begin{pmatrix} 1 \\ \tau_k \frac{\partial F_k}{\partial a_k} \\ \vdots \end{pmatrix} = \begin{pmatrix} 1 \\ \tau_k \frac{\partial g_{i(k)}}{\partial a_k}(E_{i(k)} - v_{\mathrm{sn}})/C_{\mathrm{m}} \\ \vdots \end{pmatrix}.$$

Here, $i(k)$ denotes the channel i to which the k^{th} gate belongs too.

One may give some physiological interpretation to the expression for the left eigenvector that comprises the weighting factors of the gating PRCs.

Remark 6

Positive perturbations in a gate, *i.e.*, those increasing the opening probability of a gate, will

a) advance the next spike, if the ion channel is depolarising ($E_c > v_{\mathrm{sn}}$) like a typical Na^+-channel, or
b) delay the next spike, if the ion channel is hyperpolarising ($E_c < v_{\mathrm{sn}}$) like the typical K^+-channel.

Perturbations from gating kinetics with

c) strong driving force, $(v_{\mathrm{sn}} - E_i)$,
d) strong gain in conductance, $\frac{\partial g_i}{\partial a_k}$, or
e) long kinetic time scale, $\tau_k(v_{\mathrm{sn}})$,

have a larger impact on the spike time.

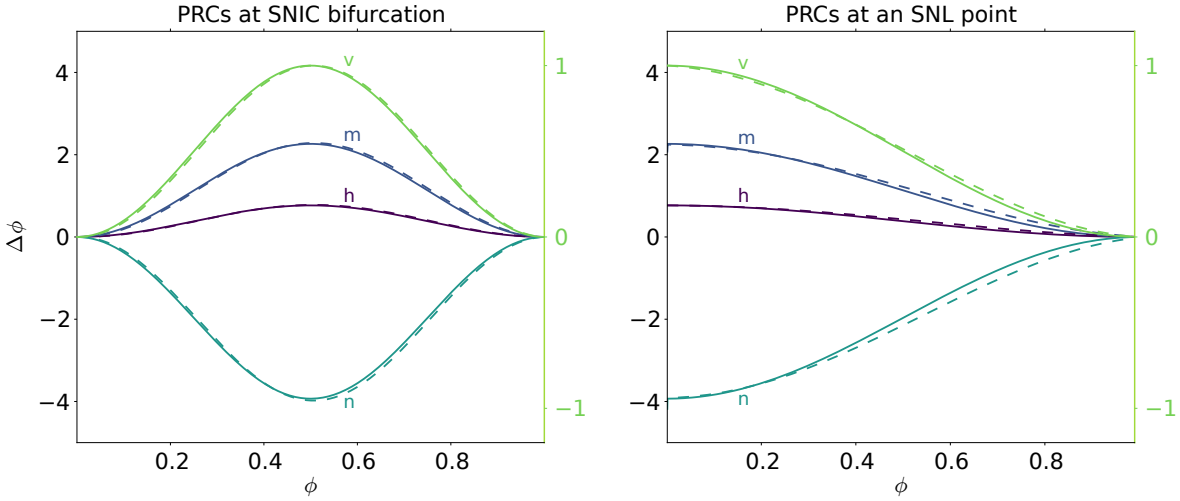

Fig. 4
Shown are numerical (dashed) and analytical (solid) gating PRCs for the Traub-Miles neuron model[38]. The parameter C_{m} was adapted to obtain SNIC and SNL spike-onset bifurcations.

Discussion

In this study, we provide an analytical tool permitting to relate perturbations induced by ion-conducting channels in a neuron's membrane to the timing of the fundamental neuronal signal — the action potential. More specifically, the analytical calculation of the phase response vector at low frequencies enables us to map high dimensional fluctuations (originating from ion channels or synaptic receptor proteins) into a phase equation from which spike statistics can be derived. Furthermore, the isochrons crossing around the centre-manifold, *i.e.*, the region where the dynamics spends most of its time, can be approximated. Remarkably, the local isochron structure is preserved not only for SNIC bifurcations, but even if the homoclinic cycle undergoes SNL (flip) bifurcations. This observation is likely to be of importance for systems close to an SNL transition, such as neurons at a particular temperature or serotonin level[31]. We found, in particular, that the relative scaling of the PRC vector components does not change at the flip bifurcation, yet the symmetry of their shape is broken.

Due to the focus on small perturbations and phase-response curves, the statements about the isochron structure at the saddle-node (*Conjecture 6*) concern the local tangent-space of the isochrons. It is not unlikely, but remains to be shown, that the whole isochron manifold near the saddle-node is equivalent to the strongly stable manifold. In this case, also the local isochron curvature would become analytically accessible and could benefit phase-amplitude models (in which it is an important ingredient). In fact, one difference between the small- and the big-SNL point is that the isochron curvature in the latter case is much stronger. This bares consequences for the identification of complete phase-amplitude models[20,40,41]. Indeed, it has already been shown that the first higher order term in Eq. (4) involves the local isochron curvature[41]. Beyond the homoclinic orbits considered here it is also exciting to consider oscillatory behaviour originating from heteroclinic loops[42].

As stated in *Remark 3*, the semi-stable manifold and its adjoint are determined by the fraction of open channels and the derivative of the ion channel's current w.r.t. the gate at the rheobase (threshold). Analytical expressions for the scaling factors are obtainable for a general conductance-based neuron models and are intuitively interpretable, *cf. Remark. 6*. However, can they be inferred from electrophysiological data? So far, the controlled perturbations required to estimate gating PRCs have not yet been tackled experimentally. In the near future, however, new techniques such as optogenetics may facilitate the stimulation of gates. The voltage PRC, on the other hand, is experimentally accessible[24,25]. The analysis presented here

concedes an alternative approach to attain the gating PRCs: Near SNIC and SNL bifurcations, their shape is equivalent to the measurable voltage PRC. The weighting factors can be determined by a combination of pharmacology and steady-state experiments akin to the seminal experiments designed by Hodgkin and Huxley[13]. Hence, we suggest that the gating PRCs can be measured without giving controlled pulses to the gates.

In many neurons models and their two-dimensional reductions, inspection of the nullclines in the phase plane appears to suggest that the centre-manifold is parallel to the voltage. *Remark 3* highlights that such contributions are never zero, but strongly depend on the slope of the activation curves at the threshold. Interestingly, cooperative ion channel gating is one biophysical mechanism that increases this slope[43,44].

The symmetry breaking in PRC that is induced by the orbit flips at the two kinds of SNL bifurcations has first been described in a previous article[31] and the strong implications for the entrainment region and high frequency filtering of neurons (if the stimuli arrive via the voltage dimension) have been discussed *ibidem*. In some neuron models (depending on their leak conductance) the big-SNL bifurcation resides close to the neuronal oscillator's relaxation limit[45]. The PRCs of relaxation oscillators look different and the reader may consult the literature[46,47], which shows the emergence of dead-zones. The dead-zone is visible in the PRC of the big-SNL shown by a previous article[31] which depicts the case of a finite period. We note that if the limit $T_\mathrm{p} \to \infty$ at the big-SNL point is taken without going to the relaxation limit, the same PRC shape as for the small-SNL point can be recovered. In this case, also the big-SNL bifurcation can be expected to be a point of change in synchronization as well as of elevated high-frequency transfer.

Finally, as a result of the work presented in this study, the consideration of gating phase-response curves of conductance-based neuron models opens up the possibility of systematic, analytical impact and sensitivity analyses of all measures of spike train statistics that can be derived from equivalent phase equations.

Acknowledgements

This work was supported by the Federal Ministry of Education and Research Germany (BMBF grants 01GQ0901, 01GQ1403). We thank Janina Hesse for valuable assistance with the proofs, help with the numerical continuation, and comments on the manuscript.

References

1. DeFelice, L.J. (1981). Introduction to membrane noise (Plenum Press).

2. White, J.A., Klink, R., Alonso, A., and Kay, A.R. (1998). Noise from voltage-gated ion channels may influence neuronal dynamics in the entorhinal cortex. Journal of neurophysiology *80*, 262–269. Available at: http://jn.physiology.org/content/80/1/262.short [Accessed December 20, 2016].

3. White, J.A., Rubinstein, J.T., and Kay, A.R. (2000). Channel noise in neurons. Trends in neurosciences *23*, 131–137. Available at: http://www.sciencedirect.com/science/article/pii/S0166223699015210 [Accessed April 21, 2017].

4. Schreiber, S., Machens, C.K., Herz, A.V.M., and Laughlin, S.B. (2002). Energy-Efficient Coding with Discrete Stochastic Events. Neural Computation *14*, 1323–1346. Available at: http://dx.doi.org/10.1162/089976602753712963 [Accessed November 14, 2014].

5. Schneidman, E., Freedman, B., and Segev, I. (1998). Ion channel stochasticity may be critical in determining the reliability and precision of spike timing. Neural computation *10*, 1679–1703. Available at: http://ieeexplore.ieee.org/xpls/abs_all.jsp?arnumber=6790648 [Accessed January 15, 2016].

6. Schreiber, S. (2003). Influence of Ionic Conductances on Spike Timing Reliability of Cortical Neurons for Suprathreshold Rhythmic Inputs. Journal of Neurophysiology *91*, 194–205. Available at: http://jn.physiology.org/cgi/doi/10.1152/jn.00556.2003 [Accessed August 4, 2015].

7. Jones, P.W., and Gabbiani, F. (2012). Impact of neural noise on a sensory-motor pathway signaling impending collision. Journal of Neurophysiology *107*, 1067–1079. Available at: http://jn.physiology.org/cgi/doi/10.1152/jn.00607.2011 [Accessed July 5, 2017].

8. Eberhard, M.J.B., Schleimer, J.-H., Schreiber, S., and Ronacher, B. (2015). A temperature rise reduces trial-to-trial variability of locust auditory neuron responses. Journal of Neurophysiology *114*, 1424–1437. Available at: http://jn.physiology.org/lookup/doi/10.1152/jn.00980.2014 [Accessed October 28, 2015].

9. Perez Velazquez, J.L., Galán, R.F., Dominguez, L.G., Leshchenko, Y., Lo, S., Belkas, J., and Erra, R.G. (2007). Phase response curves in the characterization of epileptiform activity. Physical Review E *76*. Available at: https:

//link.aps.org/doi/10.1103/PhysRevE.76.061912 [Accessed July 5, 2017].

10. Yu, H., Dhingra, R.R., Dick, T.E., and Galán, R.F. (2017). Effects of ion channel noise on neural circuits: An application to the respiratory pattern generator to investigate breathing variability. Journal of Neurophysiology *117*, 230–242. Available at: http://jn.physiology.org/lookup/doi/10.1152/jn.00416.2016 [Accessed July 5, 2017].

11. O'Donnell, C., and Rossum, M.C.W. van (2014). Systematic analysis of the contributions of stochastic voltage gated channels to neuronal noise. Frontiers in Computational Neuroscience *8*, 105. Available at: http://journal.frontiersin.org/Journal/10.3389/fncom.2014.00105/abstract [Accessed October 31, 2014].

12. Schreiber, S., Samengo, I., and Herz, A.V. (2008). Two Distinct Mechanisms Shape the Reliability of Neural Responses. Journal of Neurophysiology *101*, 2239–2251. Available at: http://jn.physiology.org/cgi/doi/10.1152/jn.90711.2008 [Accessed March 9, 2017].

13. Hodgkin, A.L., and Huxley, A.F. (1952). A quantitative description of membrane current and its application to conduction and excitation in nerve. The Journal of physiology *117*, 500. Available at: http://www.ncbi.nlm.nih.gov/pmc/articles/pmc1392413/ [Accessed September 29, 2016].

14. Rinzel, J., and Ermentrout, G.B. (1998). Analysis of neural excitability and oscillations. In Methods in neuronal modeling, C. Koch and I. Segev, eds. (MIT Press), pp. 251–291.

15. Tuckwell, H.C. (1989). Stochastic processes in the neurosciences (Philadelphia, Pa: Society for Industrial; Applied Mathematics).

16. Fox, R.F., and Lu, Y.-n. (1994). Emergent collective behavior in large numbers of globally coupled independently stochastic ion channels. Physical Review E *49*, 3421–3431. Available at: http://link.aps.org/doi/10.1103/PhysRevE.49.3421 [Accessed October 29, 2014].

17. Orio, P., and Soudry, D. (2012). Simple, Fast and Accurate Implementation of the Diffusion Approximation Algorithm for Stochastic Ion Channels with Multiple States. PLoS ONE *7*, e36670. Available at: http://dx.doi.org/10.1371/journal.pone.0036670 [Accessed October 29, 2014].

18. Linaro, D., Storace, M., and Giugliano, M. (2011). Accurate and Fast Simulation of Channel Noise in Conductance-Based Model Neurons by Diffusion Approximation. PLoS Comput Biol *7*, e1001102. Available at: http://dx.doi.org/10.1371/journal.pcbi.1001102 [Accessed October 29, 2014].

19. Winfree, A.T. (2001). The Geometry of Biological Time (Springer Science & Business Media).

20. Wedgwood, K.C., Lin, K.K., Thul, R., and Coombes, S. (2013). Phase-Amplitude Descriptions of Neural Oscillator Models. Journal of Mathematical Neuroscience *3*, 2. Available at: http://www.ncbi.nlm.nih.gov/pmc/articles/PMC3582465/ [Accessed December 15, 2014].

21. Teramae, J.-n., Nakao, H., and Ermentrout, G. (2009). Stochastic Phase Reduction for a General Class of Noisy Limit Cycle Oscillators. Physical Review Letters *102*, 194102. Available at: http://link.aps.org/doi/10.1103/PhysRevLett.102.194102 [Accessed December 15, 2014].

22. Schleimer, J.-H., and Stemmler, M. (2009). Coding of Information in Limit Cycle Oscillators. Physical Review Letters *103*, 248105. Available at: http://link.aps.org/doi/10.1103/PhysRevLett.103.248105 [Accessed November 17, 2014].

23. Lazar, A.A. (2010). Population Encoding With Hodgkin–Huxley Neurons. IEEE Transactions on Information Theory *56*, 821–837. Available at: http://ieeexplore.ieee.org/lpdocs/epic03/wrapper.htm?arnumber=5420291 [Accessed September 6, 2016].

24. Netoff, T.I. (2004). Synchronization in Hybrid Neuronal Networks of the Hippocampal Formation. Journal of Neurophysiology *93*, 1197–1208. Available at: http://jn.physiology.org/cgi/doi/10.1152/jn.00982.2004 [Accessed July 19, 2017].

25. Galán, R.F., Ermentrout, G.B., and Urban, N.N. (2005). Efficient Estimation of Phase-Resetting Curves in Real Neurons and its Significance for Neural-Network Modeling. Physical Review Letters *94*. Available at: http://link.aps.org/doi/10.1103/PhysRevLett.94.158101 [Accessed July 9, 2015].

26. Ermentrout, B. (1996). Type I membranes, phase resetting curves, and synchrony. Neural computation *8*, 979–1001. Available at: http://www.mitpressjournals.org/doi/abs/10.1162/neco.1996.8.5.979 [Accessed January 23, 2017].

27. Pikovsky, A., Rosenblum, M., and Kurths, J. (2003). Synchronization: A Universal Concept in Nonlinear Sciences (Cambridge University Press).

28. Brown, E., Moehlis, J., and Holmes, P. (2004). On the Phase Reduction and Response Dynamics of Neural Oscillator Populations. Neural Computation *16*, 673–715. Available at: http://dx.doi.org/10.1162/089976604322860668 [Accessed December 3, 2014].

29. Izhikevich, E.M. (2007). Dynamical Systems in Neuroscience (MIT Press).

30. Ermentrout, G., and Kopell, N. (1986). Parabolic Bursting in an Excitable System Coupled with a Slow Oscillation.

SIAM Journal on Applied Mathematics *46*, 233–253. Available at: http://epubs.siam.org/doi/abs/10.1137/0146017 [Accessed January 23, 2017].

31. Hesse, J., Schleimer, J.-H., and Schreiber, S. (2017). Qualitative changes in phase-response curve and synchronization at the saddle-node-loop bifurcation. Physical Review E *95*. Available at: http://link.aps.org/doi/10.1103/PhysRevE.95.052203 [Accessed May 4, 2017].

32. Schecter, S. (1987). The Saddle-Node Separatrix-Loop Bifurcation. SIAM Journal on Mathematical Analysis *18*, 1142–1156. Available at: http://epubs.siam.org/doi/abs/10.1137/0518083 [Accessed April 1, 2015].

33. Homburg, A.J., and Sandstede, B. (2003). Homoclinic and heteroclinic bifurcations in vector fields. Journal. Available at: http://www.dam.brown.edu/people/sandsted/publications/survey-homoclinic-bifurcations.pdf [Accessed April 30, 2015].

34. Winfree, A.T. (1974). Patterns of phase compromise in biological cycles. Journal of Mathematical Biology *1*, 73–93. Available at: http://www.springerlink.com/index/0668278661N54486.pdf [Accessed June 21, 2017].

35. Osinga, H.M., and Moehlis, J. (2010). Continuation-based Computation of Global Isochrons. SIAM Journal on Applied Dynamical Systems *9*, 1201–1228. Available at: http://epubs.siam.org/doi/10.1137/090777244 [Accessed June 12, 2017].

36. Kuramoto, Y. (1984). Chemical Oscillations, Waves, and Turbulence (Springer Science & Business Media).

37. Lapicque, L. (1907). Recherches quantitatives sur l'excitation électrique des nerfs traitée comme une polarisation. J. Physiol. Pathol. Gen. *9*, 620–635.

38. Ermentrout, B. (1998). Linearization of F-I Curves by Adaptation. Neural Computation *10*, 1721–1729. Available at: http://dx.doi.org/10.1162/089976698300017106 [Accessed February 9, 2015].

39. Kirst, C. (2012). Synchronization, Neuronal Excitability, and Information Flow in Networks of Neuronal Oscillators. Available at: http://ediss.uni-goettingen.de/bitstream/handle/11858/00-1735-0000-000D-F08D-2/kirst.pdf?sequence=1 [Accessed April 1, 2015].

40. Guillamon, A., and Huguet, G. (2009). A Computational and Geometric Approach to Phase Resetting Curves and Surfaces. SIAM Journal on Applied Dynamical Systems *8*, 1005–1042. Available at: http://epubs.siam.org/doi/abs/10.1137/080737666 [Accessed August 10, 2015].

41. Schleimer, J.-H. (2013). Spike statistics and coding properties of phase models. Available at: http://edoc.hu-berlin.de/docviews/abstract.php?id=40244 [Accessed November 14, 2014].

42. Neves, F.S., Voit, M., and Timme, M. (2017). Noise-constrained switching times for heteroclinic computing. Chaos: An Interdisciplinary Journal of Nonlinear Science *27*, 033107. Available at: http://aip.scitation.org/doi/10.1063/1.4977552 [Accessed July 19, 2017].

43. Naundorf, B., Wolf, F., and Volgushev, M. (2006). Unique features of action potential initiation in cortical neurons. Nature *440*, 1060–1063. Available at: http://www.nature.com/doifinder/10.1038/nature04610 [Accessed May 19, 2015].

44. Zarubin, D., Zhuchkova, E., and Schreiber, S. (2012). Effects of cooperative ion-channel interactions on the dynamics of excitable membranes. Physical Review E *85*. Available at: http://link.aps.org/doi/10.1103/PhysRevE.85.061904 [Accessed March 28, 2015].

45. De Maesschalck, P., and Wechselberger, M. (2015). Neural Excitability and Singular Bifurcations. The Journal of Mathematical Neuroscience (JMN) *5*. Available at: http://www.mathematical-neuroscience.com/content/5/1/16 [Accessed August 20, 2015].

46. Izhikevich, E.M. (2000). Phase equations for relaxation oscillators. SIAM Journal on Applied Mathematics *60*, 1789–1804. Available at: http://epubs.siam.org/doi/abs/10.1137/S0036139999351001 [Accessed November 10, 2016].

47. Zhang, C., and Lewis, T.J. (2013). Phase response properties of half-center oscillators. Journal of Computational Neuroscience *35*, 55–74. Available at: http://link.springer.com/10.1007/s10827-013-0440-1 [Accessed June 6, 2017].

